Journal of Visualization, Vol. 5, No.1 (2002) 9-19

Observation of Vortex Packets in Direct Numerical Simulation of Fully Turbulent Channel Flow

Adrian, R. J.* and Liu, Z. C.*

* Laboratory for Turbulence and Complex Flow, Department of Theoretical and Applied Mechanics, University of Illinois at Urbana-Champaign, Urbana, Illinois 61801, USA.

Received 6 August 2001
Revised 5 October 2001

***Abstract*:** A number of experimental studies have inferred the existence of packets of inclined, hairpin-like vortices in wall turbulence on the basis of observations made in two-dimensional x-y planes using visualization and particle image velocimetry (PIV). However, there are very few observations of hairpins in existing three-dimensional studies made using direct numerical simulation (DNS), and no such study claims to have revealed packets. We demonstrate, for the first time, the existence of hairpin vortex packets in DNS of turbulent flow. The vortex packet structure found in the present study at low Reynolds number, Re_τ = 300, is consistent with and substantiates the observations and the results from two-dimensional PIV measurements at higher Reynolds numbers in channel, pipe and boundary layer flows. Thus, the evidence supports the view that vortex packets are a universal feature of wall turbulence, independent of effects due to boundary layer trips or critical conditions in the aforementioned numerical studies. Visualization of the DNS velocity field and vortices also shows the close association of hairpin packets with long low-momentum streaks and the regions of high Reynolds shear stress.

***Keywords*:** wall turbulence, wall eddies, structure, hairpin vortices, hairpin vortex packets, direct numerical simulation.

1. Introduction

Despite the passage of nearly one-half century since Theodorsen's (1952) proposal that hairpin vortices constitute one of the primary flow mechanisms of wall turbulence, the existence and importance of hairpin (or horseshoe) vortices remain unsettled subjects. Opinions in the community that studies wall turbulence range from comfortable acceptance of the hairpin paradigm to non-acceptance. Among those who do allow for hairpins in the mechanical picture of wall turbulence there is sometimes serious doubt about their importance, either as stress-associated events or as mechanisms that lead to the formation of events that are important to the creation of turbulent stresses. Clearly, this situation derives from a lack of convincing evidence, especially at high Reynolds number. The difficulty lies partly in the full three-dimensionality of the hairpin structure, partly in the problem of defining a vortex, and partly in the multi-scale complexity of these flows.

In his exhaustive study of the structure of wall turbulence, Robinson (1991) identified arches of vorticity and long regions of quasi-stream-wise vorticity, but stopped short of embracing the view that these elements were connected in the form of hairpins. On the basis of flow visualization of boundary layers using smoke and a laser light sheet in a low speed wind tunnel, Head and Bandyopadhyay (1981) concluded that the boundary layer flow is full of hairpin vortices. They rose from the wall with an inclination approximately 45° to the wall and a width of about one hundred viscous wall units. Smith and co-workers (1984, 1991) have also visualized patterns that appeared to be hairpins with H_2 bubbles and dyes, but doubts always lingered because the vorticity could not be measured in the visualizations. Recently, Chacin et al. (1996) have reported observing three-dimensional hairpin

shapes in turbulent channel flow simulated by DNS, providing some of the best evidence to date for the existence of such structures, albeit at low Reynolds number.

Contemporaneously, experimental and numerical studies by the present authors and co-workers have lead to a structural model in which an important element of the turbulent wall layer is not just the hairpin vortex, but vortices that are grouped together in stream-wise-aligned packets that grow upwards at a characteristic angle with respect to the wall in the range of g = 5-15°, c.f. Fig. 1. A packet exists if the vortices within it propagate with small velocity dispersion, so that their spatial arrangement has a long lifetime. The vortices in these packets may be classified as hairpins, provided that a sufficiently liberal interpretation is given to the term. Thus, while the packet in Fig. 1 is perfectly symmetric, most vortices that occur in fully turbulent flows are asymmetric with legs of unequal strength, and they are often distorted by the motions of other vortices. Their coherent alignment creates an induced backflow region inside the packet that is much longer than the backflow induced by a single vortex, thus explaining the extraordinarily long correlation length of the stream-wise momentum, as observed by Grant (1958) and Townsend (1976). The grouping of the vortices also explains the occurrence of multiple second-quadrant events in turbulent bursts, as documented by Bogard and Tiederman (1986), Luchik and Tiederman (1987) and Tardu (1995), and the lift-up/oscillation/violent ejection sequence of events observed in a turbulent burst (c.f. Robinson, 1991 for a review).

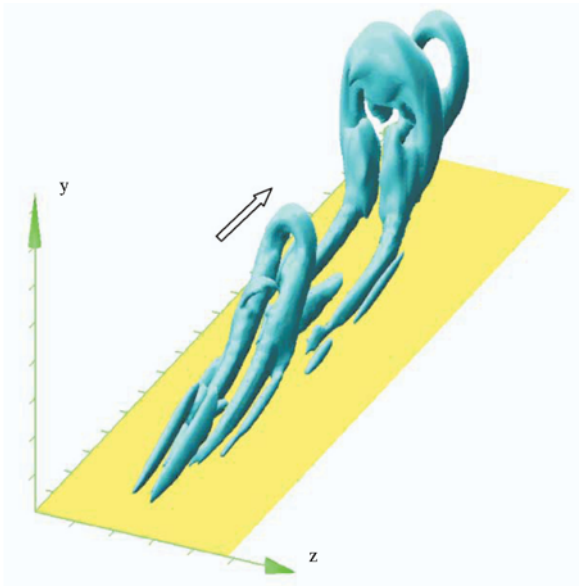

Fig. 1. The hairpin vortex packet that evolves from a symmetric primary hairpin as computed by DNS in Re_t = 150 channel flow (from Zhou et al., 1999). The surfaces are contours of the swirling strength.

The hairpin vortex packet paradigm finds precedence in the earlier pioneering studies by Head and Bandyopadhyay (1981) and Smith (1984). Both observed two or more hairpins occurring in stream-wise alignment in natural turbulent boundary layers. Smith's (1984) H_2-bubble visualizations were at low Reynolds number close to the wall, while Head and Bandyopadhyay's (1981) observations of inclined packets were principally at the interface between a smoke-filled, moderate Reynolds number boundary layer and the clean free stream.

By examining the signatures of the hairpins vortices, the recent two-dimensional PIV experiments of Adrian, Meinhart and Tomkins (2000) (hereafter referred to as AMT 2000) reveal that moderate Reynolds number turbulent wall flow is densely populated with hairpin-shaped vortices grouped into coherent vortex packets. Two-dimensional PIV experiments find multiple zones of nearly uniform stream-wise momentum, suggesting that the boundary layer is made up of a hierarchy of vortex packets. The younger packets are located near the wall, while the older packets are larger and occupy space farther away from the wall. Wide-angle, two-dimensional PIV measurements at moderate Reynolds number document the geometry of full vortex packets. Their shapes vary, but the characteristic angle of growth is common, and the experiments provide evidence that the vortex packets are a frequently occurring coherent structure.

Smith et al. (1991) offer a model that explains the mechanisms of self-induction that can lead a single hairpin to form a packet of hairpins and Zhou et al. (1996, 1998, 1999) independently found the process of auto-generation of new vortices by numerical simulation of a single vortex at low Reynolds number (Re_τ = 150) in an otherwise clean turbulent channel flow. An initial hairpin-like structure generated by stochastic estimation based on two-point correlation of velocities was put into a mean turbulent velocity profile and allowed to evolve. When the strength of the initial structure was above a threshold, it developed and formed a primary hairpin, and subsequently generated secondary and tertiary hairpins and later a downstream hairpin, as shown in Fig. 1. These hairpin vortices organize themselves into a coherent packet aligned in the stream-wise direction. The complete Navier-Stokes mechanisms for the generation of vortex packets agreed with the most of the model of Smith et al. (1991), although Zhou et al. (1996, 1998, 1999) also predicted a threshold intensity of the primary vortex that is required to initiate auto-generation.

Although the PIV experiments (at moderate Reynolds number and in several different flow apparatus) indicate frequent occurrence of vortex packets in fully turbulent flows, and the numerical/theoretical studies of the evolution of a single hairpin suggest mechanisms by which vortex packets can be formed, there are still some missing threads in the fabric of the evidence. First, the simulations of Zhou et al. (1996, 1998, 1999) were at a Reynolds number that was close to transition, raising questions about the extension of these concepts to higher Reynolds number. Second, hairpin packets have not been reported in direct numerical simulations of fully turbulent flow. This is not, perhaps, surprising, since even the visualization of a single hairpin in the complex environment of a fully turbulent flow is a careful study that has only been accomplished recently (Chacin et al., 1996). Even so, it is important to clarify this question. If hairpin vortex packets cannot be found in fully turbulent DNS, it could mean that the inference of hairpins from the two-dimensional PIV data is incorrect, or that imperfections in real flow fields (wall roughness, vibrations, inlet disturbances, etc.) favor the production of packets, while the perfect conditions of direct numerical simulations discriminate against their formation. On the other hand, if hairpin packets can be found in fully turbulent direct numerical simulations, the case for their universal nature, independent of secondary factors, is strengthened considerably.

The present DNS of fully developed turbulent channel flows has been performed at Re_τ = 300, twice the Reynolds number of the Zhou et al. (1996, 1998, 1999) simulations. We find that packets with mostly asymmetric hairpin vortices can be observed in both halves of the channel flow for every realization of the present DNS. They occur frequently in both space and time. The observations are consistent with previous two-dimensional PIV experiments in boundary layer and channel flows and with the DNS study of the growth of a packet out of an individual hairpin. The three-dimensional capability of DNS data provides three-dimensional information for the packet structure and characteristics and a clearer picture than the two-dimensional visualizations. The present DNS study also observes a close association of packets with Q2 and Q4 events, long low-momentum streaks and the generation to Reynolds stress.

2. Direct Numerical Simulation

The simulation of fully developed channel flow was performed by solving the full three-dimensional time-dependent Navier-Stokes equations using the pseudo-spectral code originally developed by Lyons et al. (1991). The Reynolds number, Re_τ, based on the half channel height, h, and the friction velocity, $u_\tau = \sqrt{(\nu \partial U/\partial y|_{\text{wall}})}$, was 300, where ν was the kinematic viscosity. Periodic boundary conditions were imposed in the stream-wise and span-wise directions, and no-slip and no-penetration conditions held at both walls. The pseudo-spectral method used Fourier series expansions in the stream-wise (x) and span-wise (z) directions and Chebychev polynomial series expansions in the wall-normal (y) direction, and spatial derivatives of the velocity field were computed in spectral space. The algorithm made use of a time-splitting technique in three fractional steps to compute the non-linear convective term, the pressure term and the viscous term of the Navier-Stokes equations. The details of the algorithm have been described in Lyons et al. (1991).

The computational domain in the stream-wise, span-wise and wall-normal directions was $3800^+ \times 1900^+ \times 600^+$ in wall units (ν/u_τ) with grid numbers of $256 \times 256 \times 129$, giving approximately 8.5 million data points. The grid spacing in wall units was 14.9 and 7.49 in x^+ and z^+, and it ranged from 0.09-7.36 in y^+.

3. Evolution of Vortex Packets at $Re_t = 300$

The evolution of a single hairpin into a packet of vortices has been computed for the present Reynolds number using procedures identical to those described in Zhou et al. (1996, 1998, 1999). Here, and throughout this paper, we visualize vortices using level surfaces of the swirling strength, as defined in Zhou et al. (1996, 1998, 1999). This flow pattern analysis is based on the critical point concepts of Perry and Chong (1987), Chong et al (1990). The eigenvalues of the velocity gradient tensor of incompressible flow for every grid point in the flow field are obtained by solving the characteristic equation, $l^3 + Ql + R = 0$, where Q and R are the tensor invariants that determine the local flow pattern. The discriminant is $D = (27/4)\,R^2 + Q^3$. For $D \le 0$ eigenvalues are real. For $D > 0$ there are one real and two complex conjugate eigenvalues. In this case the flow pattern exhibits stable focus/stretching ($R < 0$) or unstable focus/compressing ($R > 0$). Zhou et al. (1996, 1998, 1999) defined the swirling strength to be the imaginary part of the complex conjugate eigenvalue, l_{ci}, a new kinematic quantity representing swirling rate around the axis of principal stretching/compression. Surfaces of non-zero constant swirling strength are much like surfaces of constant enstrophy, except that they exclude pure shear, which implies zero swirling strength. The use of swirling strength has the main advantage of avoiding regions of shearing motions that have small swirl, but strong vorticity.

The computations at $Re_t = 300$ began with an eddy, shown in Fig. 2, that was found by stochastically estimating the conditional average of the flow field surrounding a second-quadrant (Q2) event at $y^+ = 49$. Due to sampling error in forming the two-point spatial correlations needed for the stochastic estimate, the initial eddy contained an asymmetry of approximately 5 per cent with respect to reflections about the x-y mid-plane. The initial condition used by Zhou et al. (1996, 1998, 1999) was perfectly symmetric, so it led to the symmetric pattern in Fig. 1. For comparison, the initial condition for the $Re_t = 300$ computation was also symmetrized about the x-y plane, and it was found that a pattern similar to Fig. 1 resulted. Doubling the Reynolds number produced no significant change in the pattern of the eddies in the hairpin packet.

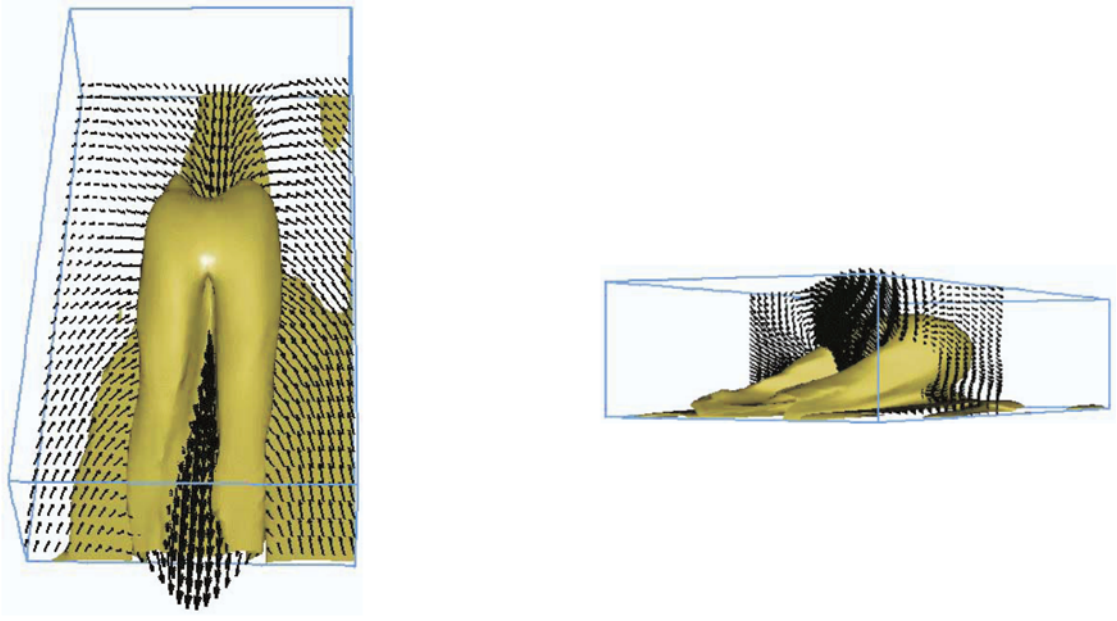

Fi g. 2. Initial vortex found by conditionally averaging the velocity field around a Q2 event located at $y^+ = 50$ in a $Re_t = 300$ channel flow. The surfaces are contours of the swirling strength.

As shown previously (Zhou et al., 1999), asymmetric events grow more rapidly than symmetric events, so they are likely to be the most common form found in natural wall turbulence. To explore this effect the residual asymmetry in Fig. 2 was allowed to remain, with the result that the surprisingly complicated packet shown in Fig. 3 evolved out of the relatively minor asymmetry. This packet contains many hairpins that have the form of a cane or a one-legged hairpin. It gives clear meaning to the liberal sense in which hairpins are defined by Zhou et al. (1999).

The growth angle of the packet is about $g = 15^{\circ}$, similar to the results for the symmetric packets. It contains about five clear hairpins, plus several that are only partially formed. As the evolution of the packet progresses, a considerable amount of interaction occurs by self-induction, leading to many small-scale vortices that create a complicated and apparently chaotic picture that makes identification of the main hairpins difficult. Nevertheless, they can be seen clearly without need of special eduction methods. In fact, eduction is an inferior method of visualizing these structures, because it smoothes the data too much. For this reason, we use visualization of individual structures throughout this paper as the preferred method of demonstrating properties of the packets.

It must be emphasized that the principal difference between the packets in Fig. 2 and Fig. 3 is due to the initial asymmetry, and not the higher Reynolds number.

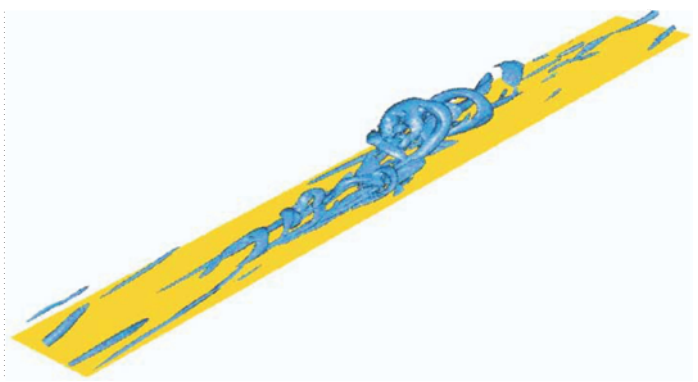

Fig. 3. The hairpin vortex packet that evolves in Re_t = 300 channel flow from the slightly asymmetric primary hairpin in Fig. 2. t^+ = 250. Note the complexity of this packet relative to the packet in Fig. 1. An animation of the evolution from the initial disturbance can be seen at http://www.ltcf.tam.uiuc.edu. The surfaces are contours of the swirling strength.

4. Hairpin Vortex Packets in Fully Turbulent Flow

We next consider the results of simulating the fully turbulent flow in the channel. A portion of a typical turbulent realization is visualized on a sub-domain having dimensions $950^+ \times 475^+$, and half of the channel height, 300^+ using iso-surfaces of enstrophy, $|w|$, in Fig. 4(a) and swirling strength, I_{ci}, in Fig. 4(b). The volume of the sub-domain in Fig. 4 is 1/32 of the volume of the whole computational domain. Comparison of Fig. 4(a) and Fig. 4(b) shows that swirling strength captures vortices that contain concentrated vorticity, but discards the shearing motions, making

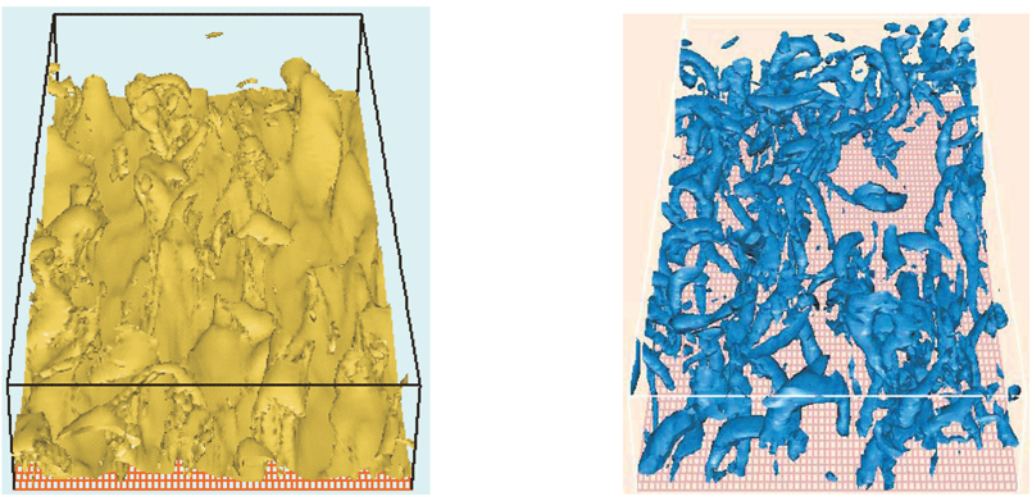

Fig. 4. A typical turbulent realization visualized on a sub-domain having dimensions (L^+_x, L^+_y, L^+_z) = (950, 300, 475). (a) Iso-surfaces of the enstrophy, Iwl; (b) iso-surfaces of the swirling strength, I_{ci}.

visualization much easier. In the view looking downstream from above, vortices are seen to concentrate in groups that are aligned in the stream-wise direction. Two groups reside in the middle half of the span, and there are indications of a portion of a group at the left and right edges. The character of the vortices in these groups is difficult to determine from this view.

Figure 5(a) is a side-view that shows quasi-streamwise vortices extending along the wall and gradually tilting up at an angle of 30-45 degrees. This pattern recurs frequently, and it is easy to conclude that it is strong characteristic of the flow. The inclined vortices may be hairpin legs. In Fig. 5(b) hairpin heads (or 'arches', in the terminology of Robinson, 1991) can be seen, and some of them are clearly attached to inclined vortices, forming a cane or a hairpin. The heads of some of the inclined vortices may not visible because their swirling strength falls below the value used to render the images. Thus, one sees many inclined vortices that appear to terminate in the flow. Decreasing the swirling strength level used for the visualization makes the heads of these inclined vortices visible, but it also increases the background clutter, making it difficult to see the other structures. Hence, the value of swirling strength used in the volume renderings is a compromise.

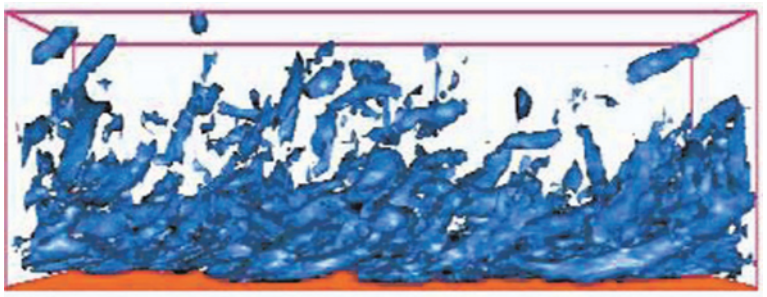

(a)

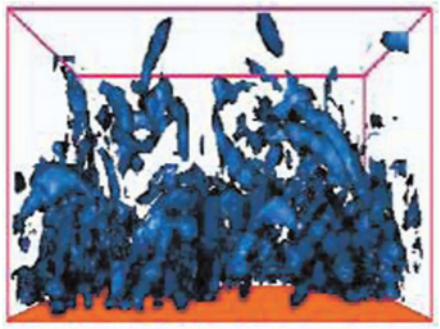

(b)

Fig. 5. (a) Side view of the channel flow in Fig. 4; (b) end view. The visualization is done using contours of the swirling strength, as in Fig. 4(b).

Despite the clarity achieved by visualizing the vortices using the swirling strength (compare Fig. 4(a) to 4(b)), the three-dimensional visualizations in Fig. 4(b) and Fig. 5 are disappointingly difficult to interpret. To make the most reliable identification of a hairpin, we have found it best to first visualize the two-dimensional flow in the *x*-*y* plane, as in Fig. 6. This also makes it possible to relate the DNS flow fields to the results of other studies such as the planar PIV study in AMT (2000) and the planar visualization of DNS data in Guenther et al. (1998). Signatures of hairpins can be observed in the typical flow field shown in Fig. 6. Hairpin heads appear as span-wise vortices in the *x*-*y* plane roughly located on a line inclined about 11 degrees with the wall. Below the vortex heads a strong low-momentum flow occurs as a result of the collective pumping effect by the hairpin legs and heads in the packet. The low-momentum fluid from each hairpin meets the high momentum fluid from the outer region of the channel and forms stagnation points and a shear layer.

The structure in Fig. 6 is a hairpin packet comprised of at least four hairpin vortices. A three-dimensional schematic of the hairpin vortex packet paradigm is shown in Fig. 7(a). The reader can see how an *x*-*y* section though the middle of a three-dimensional packet like that depicted in Fig. 7(a) would result in a pattern like that in Fig. 6. The younger hairpins in a packet are the smaller ones that are located upstream with smaller inclination to the wall; the larger hairpins that are located downstream with larger tilt angles are the older ones. Packet structures occur frequently throughout the DNS database in a region between the wall and about 0.6*h*. They are typically about 3-6*h* long in the stream-wise direction. They occur less frequently above 0.6*h*, but they can sometimes reach beyond the center of the channel. The alignment of the vortices allows the back-induced flow from each hairpin to feed into the succeeding hairpin, creating long, low-momentum streaks. These streaks have also been observed in the *x*-*z* plane with similar length in stream-wise direction (Liu et al., 1996). The spanwise spacing of neighboring streaks close to the wall, ranging from 100 to 200 wall units, clearly associates them with the classical low speed streaks first observed by Kline et al. (1967). The spanwise spacing grows linearly with distance from the wall.

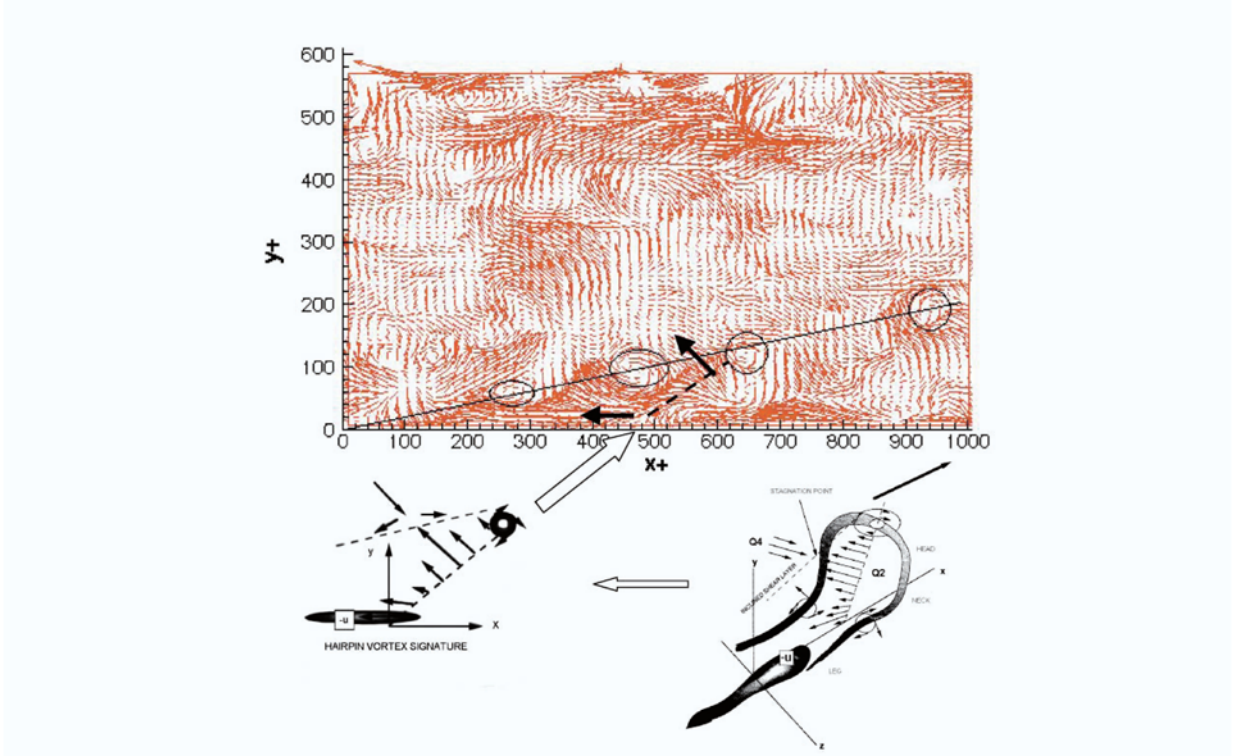

Fig. 6. A typical *x*-*y* cross-section of the channel flow. Note the presence of several patterns that match the hairpin vortex signature consisting of a vortex head atop an incline region of Q2 vectors lying downstream of a region of Q4 vectors that stagnate against the Q2 flow. One of the patterns is highlighted.

Having unambiguously located the heads of the hairpins in a view such as Fig 6, it is possible to return to the three-dimensional visualization and highlight those vortices, as shown in Fig. 7(b). The pattern of a packet of growing hairpin vortices now becomes clear. There are still many vortices cluttering the background, but a succession of increasingly taller and wider hairpins is quite evident. The view in Fig. 7(c) makes the spanwise growth more evident. Applying this method to many different samples from the DNS database consistently yields similar results. In this way, the coherent hairpin vortex pattern can be extracted from the complex pattern of vortices in the background. One can ask where these other vortices arise. One answer lies in Fig. 3 which shows that the internal dynamics of an auto-generating hairpin packet are capable of creating complexity that is similar to that observed in the fully turbulent channel flow. In addition, the large packets move faster than the smaller packets, so that there is a continual series of vortex cut-and-connect interactions as the younger hairpins are overrun by the older ones.

The three-dimensional pattern in Fig. 7(c) provides a fundamental insight into the nature of hairpin packet growth. The mean width of the young packet is about 100-200 wall units, and the hairpin heads grow wider at an angle of 10-12° in the spanwise direction. This angle is nearly the same as the rate of growth in the wall-normal direction, suggesting that the growth of the hairpins is approximately self-similar as they age. The logarithmic variation of the mean velocity is probably associated with the length scale (width or height) increasing with y, causing the back-induced velocity, and hence the mean velocity gradient, to decrease as y^{-1}.

By examining packets at subsequent times we have found that whole packets convect downstream as a coherent structure with little dispersion, so that they exist as slowly evolving patterns for many hundred viscous time scales. The convection velocity of the packet in Fig. 7 is about $12u_t$, or 76% of the bulk velocity of the channel.

Tomkins (1997) and Tomkins and Adrian (1999) showed that as a packet grows larger a new, smaller packet very often occurs below it. A similar phenomenon occurs in the DNS, c.f. Fig. 6. In this manner, a hierarchy of packets forms with older packets residing above younger ones.

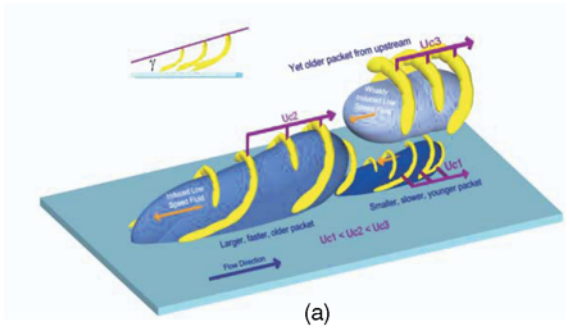

(a)

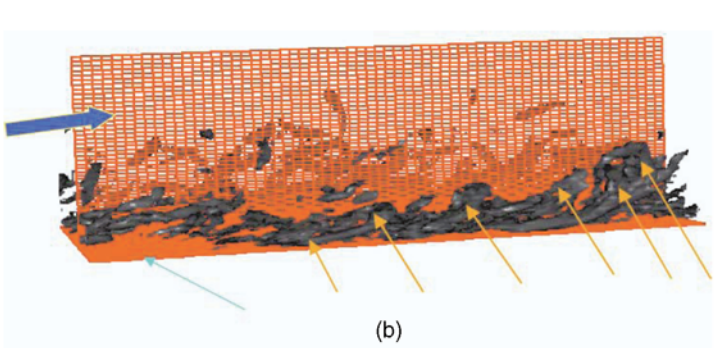

(b)

(c)

Fig. 7. (a) Schematic of the hairpin vortex packet model (from Adrian et al., 2000); (b) hairpins identified by inspecting the side view of the velocity field in Fig. 6 using the template provided by the hairpin vortex signature; (c) oblique view of the hairpin packet formed from the vortices found in Fig. 6(b). Hairpins in the packet are highlighted in red.

Figure 8 shows the eddy structure across the entire channel. Hairpin packets can be seen growing from each wall, and interacting near the centerline. This illustrates a fundamental difference between boundary layer turbulence and channel flow turbulence. In the former, one only has packets growing up from the wall, with no interference from other vortices at the outer edge. In channel flow, the packets experience perturbations from their natural, auto-induced growth mechanism due to vortices from the other side of the channel. These interactions increase the complexity of the pattern, making channel flow somewhat more difficult to visualize and understand.

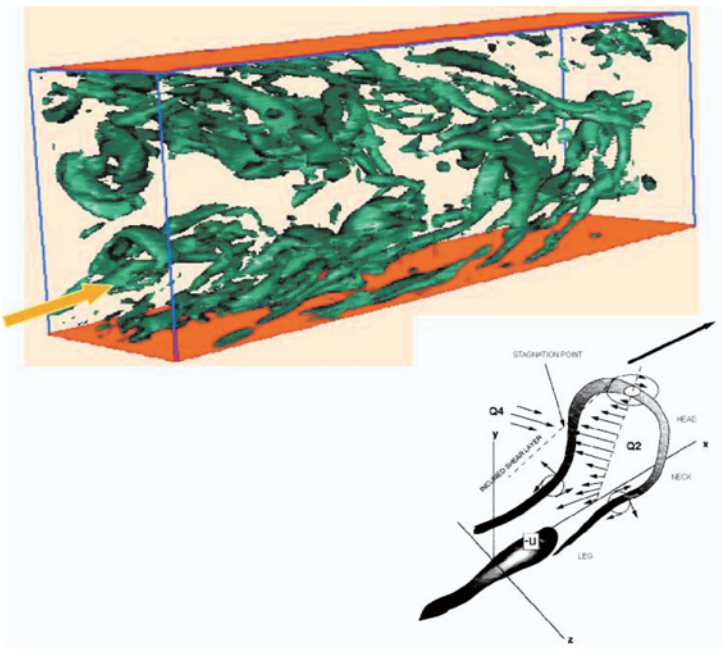

Fig. 8. Contours of swirling strength show hairpin packets growing from both the top and bottom walls of the channel.

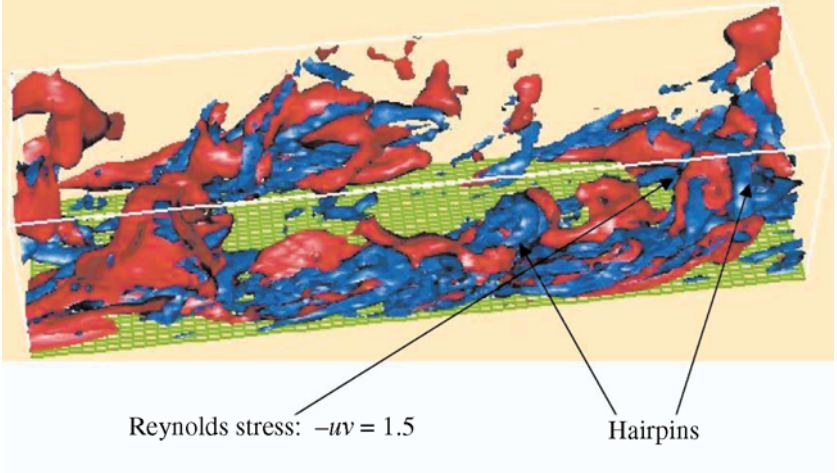

Fig. 9. The alignment of hairpins in the packets creates long streaks of Reynolds shear stress, accounting for much of the total turbulent friction.

Inboard of a hairpin the quasi-stream-wise legs and the hairpin head pump low-momentum fluid away from the wall, creating the ejection events. On the outboard sides of the legs and above the head high momentum fluid is pumped downward from the outer region of the channel, and sweeps, i.e. Q4 events, occur. These Q2 and Q4 events contribute strongly to the mean Reynolds stress. Indeed, they appear to be the main source of turbulent friction in wall turbulence. The collective actions of the Q2 and Q4 events from successive hairpins in the packets create long streaks of large Reynolds shear stress. Thus, the shear stress contours, labeled red in Fig. 9, form long streaky regions that lie inside and outside of the packet. This may explain recent observations by Hommema (2001) that show that a large fraction of the turbulent shear stress comes from very low wave numbers in the streamwise co-spectrum of u-v.

5. Conclusions

After sufficient time has elapsed, small asymmetry in the initial pattern used to seed the growth of an auto-generating hairpin packet leads to a complex pattern bordering on chaos. Earlier work with asymmetric initial conditions in AMT (2000) showed that the preferred form of hairpin vortex is the cane shape, rather than a symmetric hairpin. But, by extending the time of the computation, one finds that both canes and symmetric hairpins occur in a very complicated pattern. This pattern bears many similarities to the patterns observed in fully turbulent simulations, suggesting that much of the randomness in channel flow turbulence is actually inherent in the dynamics of hairpin vortex packets.

The present study presents results that provide clear evidence for the existence of hairpin packets in fully turbulent DNS channel flow. Although a few previous DNS studies showed the existence of individual hairpin vortices (c.f. Chacin et al., 1996), the present study, for the first time, reveals the existence and the frequent occurrence of hairpin packets in DNS of wall turbulence. The present observations of the structure and the characteristics of the coherent packets are consistent with and substantiate the previous observations from two-dimensional PIV experiments by AMT (2000) and Tomkins and Adrian (1999) for boundary layer flows, and the evolution study in DNS channel flow by Zhou et al. (1999).

Acknowledgments

This work was supported by grants from the United States National Science Foundation, NSF ATM 95-22662 and the Office of Naval Research, N00014-99-1-0188. The support and computational facilities of University of Illinois National Center for Supercomputer Applications, Urbana-Champaign are gratefully acknowledged.

References

Adrian, R. J., Balachandar, S. and Tomkins, C. D., The Structure of Vortex Packets in Wall Turbulence, AIAA 98-2962 (1998).

Adrian, R. J., Meinhart, C. D. and Tomkins, C. D., Vortex Organization in the Outer Region of Turbulent Boundary Layers, Journal of Fluid Mechanics, 422 (2000), 1-53.

Bogard, D. G. and Tiederman, W. G., Burst Detection with Single-Point Velocity Measurements, Journal of Fluid Mechanics, 162 (1986), 389-413.

Chacin, J. M., Cantwell, B. J. and Kline, S. J., Study of Turbulent Boundary Layer Structure Using the Invariants of the Velocity Gradient Tensor, Experimental Thermal and Fluid Science, 13 (1996), 308-317.

Chong, M. S., Perry, A. E. and Cantwell, B. J., A General Classification of Three-Dimensional Flow Fields, Physics of Fluids, A2 (1990), 765-777.

Grant, H. L., The Large Eddies of Turbulent Motion, Journal of Fluid Mechanics, 4 (1958), 149.

Guenther, A., Papavassiliou, D. V., Warholic, M. D. and Hanratty, T. J., Turbulent Flow in a Channel at a Low Reynolds Numbers, Experiments in Fluids, 25 (1998), 503-511.

Head, M. R. and Bandyopadhyay, P. B., New Aspects of Turbulent Boundary-Layer Structure, Journal of Fluid Mechanics, 107 (1981), 297-338.

Hommema, S. E., Very Large Scale Motion in Wall-Bounded Turbulence, Ph.D. thesis, University of Illinois, Urbana, Illinois, USA (2001).

Kline, S. J., Reynolds, W. C., Schroub, F. A. and Rundstadler, P. W., The Structure of Turbulent Boundary Layers, Journal of Fluid Mechanics, 12 (1967), 741.

Liu, Z. C., Adrian, R. J. and Hanratty, T. J., A Study of Streaky Structure in a Turbulent Channel Flow with Particle Image Velocimetry, 8th International Symposium on Applications of Laser Techniques to Fluid Mechanics, (Lisbon), (1996), 17.1.1-17.1.9.

Luchik, T. S. and Tiederman, W. G., Time-Scale and Structure of Ejections and Bursts in Turbulent Channel Flows, Journal of Fluid Mechanics, 174 (1987), 529-552.

Lyons, S. L., Hanratty, T. J. and McLaughlin, J. B., Large-Scale Computer Simulation of Fully Developed Turbulent Channel Flow with Heat Transfer, International Journal of Numerical Methods in Fluids, 13 (1991), 999-1028.

Meinhart, C. D. and Adrian, R. J., On the Existence of Uniform Momentum Zones in a Turbulent Boundary Layer, Physics of Fluids, 7 (1995), 694-696.

Perry, A. E and Chong, M. S., A Description of Eddying Motions and Flow Patterns Using Critical-Point Concepts, Annual Reviews Fluid of Mechanics, (1987), 125-155.

Robinson, S. K., Coherent Motion in the Turbulent Boundary Layer, Annual Reviews Fluid of Mechanics, 23 (1991), 601-639.

Smith, C. R., A Synthesized Model of the Near-Wall Behavior in Turbulent Boundary Layers, Proceedings of the 8th Symposium on Turbulence (ed. Zakin, J. and Patterson, G.), (1984), 299-325, University Missouri-Rolla, Rolla, Missouri.

Smith, C. R., Walker, J. D. A., Haidari, A. H. and Sobrun, U., On the Dynamics of Near-Wall Turbulence, Philosophical Transactions of the Royal Society of London A, 336 (1991), 131-175.

Tardu, S., Characteristics of Single and Clusters of Bursting Events in the Inner Layer, Part 1: Vita Events. Experiments in Fluids, 20 (1995), 112-124.

Theodorsen, T., Mechanism of Turbulence, Proceedings 2nd Midwestern Conference on Fluid Mech., (1952), 1-19, Ohio State University, Columbus, Ohio.

Tomkins, C. D. and Adrian, R. J., Characteristics of Vortex Packets in Wall Turbulence, in Turbulence and Shear Flow Phenomena (eds. Bannerjee, S. and Eaton, J.), (1999), 31-36, Begell House, New York.

Tomkins, C. D., A Particle Image Velocimetry Study of Coherent Structures in a Turbulent Boundary Layer, M.S. thesis, (1997) University of Illinois, Urbana, Illinois, USA.

Townsend, A. A., The Structure of Turbulent Shear Flow (2nd edition), (1976), Cambridge University Press, Cambridge.

Zhou, J., Adrian, R. J. and Balachandar, S., Autogeneration of Near-Wall Vortical Structures in Channel Flow, Physics of Fluids, 8 (1996), 288-290.

Zhou, J., Adrian, R. J., Balachandar, S. and Kendall, T. M., Mechanisms for Generating Coherent Packets of Hairpin Vortices in Near-Wall Turbulence, Journal of Fluid Mechanics, 387 (1999), 353-396.

Zhou, J., Meinhart, C. D., Balachandar, S. and Adrian, R. J., Formation of Coherent Hairpin Packets in Wall Turbulence, in Self-Sustaining Mechanisms of Wall Turbulence (ed. Panton, R. L.), (1998), 109-134, Computational Mechanics Publications, Southampton, UK.

Author Profile

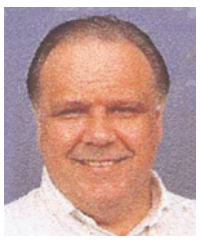

Ronald J. Adrian: He received his B.M.E. degree in Mechanical Engineering in 1967 from the University of Minnesota, his M.S. degree in Mechanical Engineering in 1969 from the University of Minnesota, and his Ph.D. degree in Physics in 1972 from the University of Cambridge. He joined the University of Illinois in 1972 where he became a full Professor in 1981. He now holds the Leonard C. and Mary Lou Hoeft Chair in Engineering and is Director of the Laboratory on Turbulence and Complex Flows in the Department of Theoretical and Applied Mechanics. His research interests are turbulence, wall turbulence, thermal convection, vortex structures, laser instrumentation and experimental fluid mechanics.

Zi-Chao Liu: He was Associate Professor at Beijing Institute of Aeronautics and Astronautics from 1979-1987 and at the Chinese Academy of Sciences in 1987. He developed laser and optical techniques in experimental fluid mechanics during visits at Princeton University, Stanford University and the University of Michigan from 1979-1982 and Essen University in Germany from 1987-1988. He was Visiting Professor and Senior Research Engineer at the University of Illinois from 1988-2000, conducting research on wall turbulence. His research interests are turbulence, direct numerical simulations of wall turbulence and vortex structures, laser techniques in fluid mechanics.